

## Scanning tunneling microscopy studies of the $\text{TiO}_2(110)$ surface: Structure and the nucleation growth of Pd

C. Xu, X. Lai, G. W. Zajac,\* and D. W. Goodman†

Department of Chemistry, Texas A&M University, College Station, Texas 77843-3255

(Received 21 April 1997; revised manuscript received 2 July 1997)

The surface structure of  $\text{TiO}_2(110)$  has been reexamined using scanning tunneling microscopy (STM), especially in terms of its temperature dependency. A dramatic topographic change was observed around 725 K, which is most likely due to the oxygen desorption into the gas phase and the simultaneous diffusion of Ti into the bulk. The atomically resolved STM images show a strong dependency on the tip composition and allow a double-bridging oxygen vacancy to be identified. The nucleation and growth of Pd on the  $\text{TiO}_2(110)$  surface have also been studied at the nucleation stage with atomic resolution. Both dimer and tetramer Pd clusters have been observed; however no single Pd atoms were detected. These results support the ‘classical’ nucleation model which assumes that only monomers are mobile, whereas dimers are stable nuclei. A marked preferential nucleation and growth of Pd clusters at step edges have also been observed. In addition to topographic structures, the local electronic properties of the Pd clusters have been studied to relate cluster structure to electronic composition. [S0163-1829(97)06243-7]

### I. INTRODUCTION

The discovery of photocatalytic activity of  $\text{TiO}_2$  electrodes for decomposing water by Fujishima and Honda,<sup>1</sup> and the strong metal/support interaction by Tauster, Fung, and Garten,<sup>2</sup> have promoted extensive studies of the  $\text{TiO}_2$  surface and its interaction with supported metal clusters. Recently, scanning tunneling microscopy (STM) has been used to study the geometric structure of  $\text{TiO}_2$  surfaces with atomic resolution.<sup>3–19</sup> Because of its high thermodynamic stability, the  $\text{TiO}_2(110)$  surface has often been chosen for these studies, although a few STM studies have been carried out on the (100) (Refs. 3–6) and (001) (Ref. 7) faces. Figure 1, which contains a schematic drawing of a  $(1 \times 1)$   $\text{TiO}_2(110)$  surface, shows both in-plane and bridging oxygen anions as well as fivefold-coordinated titanium cations at the surface. Two kinds of oxygen vacancies, missing either one bridging oxygen atom or two adjacent oxygen atoms, are indicated. The first ultrahigh-vacuum (UHV) –STM studies for this surface with atomic resolution show individual atoms ordered along the  $[11\bar{3}]$  or  $[11\bar{1}]$  directions, corresponding to the crystallographic shear directions of partially reduced  $\text{TiO}_2$  crystals.<sup>8–10</sup> Recently, STM images with atomic resolution showing individual atom rows running along the  $[001]$  direction have been reported by various groups.<sup>11–17</sup> The distance between the individual atom rows was measured to be 6.5 Å in the STM images and indicates that only one of the two ions (O and Ti) was imaged. Since all the STM images were acquired at a positive sample bias, it was assumed that the Ti cations were imaged because of the availability of the appropriate unoccupied orbitals.<sup>11–16</sup> By imaging the formate species adsorbed on the  $\text{TiO}_2(110)$  surface, Onishi and Iwasawa have verified this assignment.<sup>18</sup> Using an oxygen vacancy as a microscopic marker, Fischer *et al.*,<sup>17</sup> reassigned the bright spots in the STM image to the oxygen anions; however, this reassignment has been challenged recently by Diebold *et al.*<sup>19</sup> Using the same method (oxygen vacancy as a

marker) and backed by first-principles pseudopotential calculations to determine the state accessible for tunneling, these authors demonstrated that the Ti cations were imaged in their STM experiments. In addition to the  $(1 \times 1)$  structure, a  $(1 \times 2)$  reconstruction also has been observed based on low-energy electron diffraction (LEED) and STM studies.<sup>11–16,20</sup> There remains some controversy regarding both the forma-

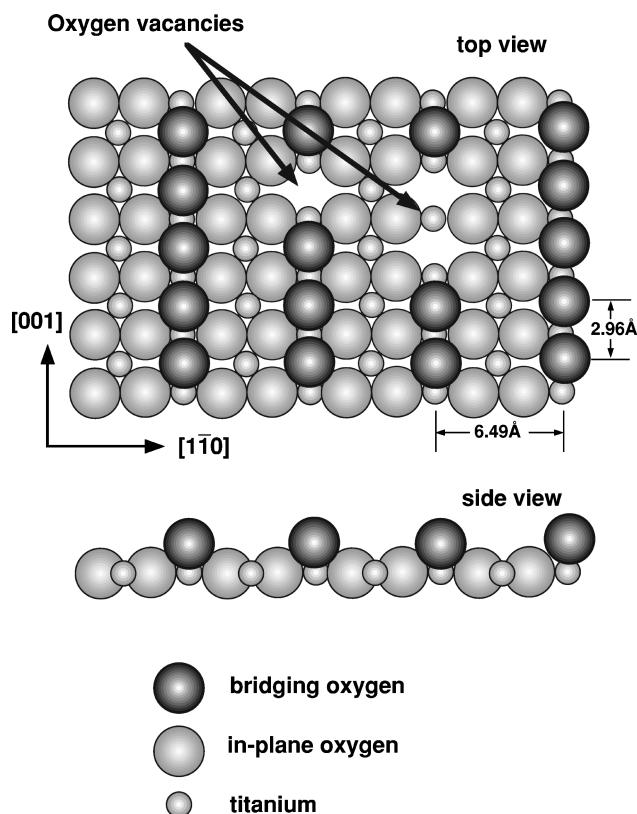


FIG. 1. Schematic drawing of the  $\text{TiO}_2(110)$  surface: top view (top) and side view (bottom). Also indicated were single and double bridging oxygen vacancies.

tion conditions and the microscopic model for the  $(1 \times 2)$  reconstruction. By annealing the sample between 730 and 880 K, Møller and Wu<sup>20</sup> obtained the  $(1 \times 2)$  reconstructed surface which then reversibly converted to a  $(1 \times 1)$  surface after further annealing to 980 K. However, various STM experiments performed by Engel and co-workers,<sup>11,14</sup> Iwasawa and co-workers,<sup>13,15</sup> and Murray, Condon, and Thornton<sup>16</sup> show only the formation of the  $(1 \times 2)$  reconstructed surface after annealing the sample to  $\sim 1200$  K. The first model proposed by Møller and Wu<sup>20</sup> for the reconstructed surface involves the removal of alternant bridging oxygen rows. Based on STM results, Szabo and Engel,<sup>14</sup> and Murray, Condon, and Thornton<sup>16</sup> have further modified this model by introducing varying degrees of relaxation of the Ti cations. Recently, Onishi and Iwasawa<sup>13</sup> have proposed a model in which the reconstruction was attributed to the formation of an added  $\text{Ti}_2\text{O}_3$  row structure. This structure was supported by STM images of the formate species<sup>18</sup> and has been further verified by Guo, Cocks, and Williams using electron-stimulated desorption ion angular distribution.<sup>21</sup>

An understanding of the nucleation and growth of metals on oxide surfaces is crucial to a number of technologies including electronic devices, catalysis, and sensors.<sup>22–24</sup> Extensive research has been devoted to the study of the nucleation and growth of metal clusters on oxide surfaces.<sup>22–24</sup> Pd supported on  $\text{TiO}_2(110)$  has been previously studied by Evans, Hayden, and Lu,<sup>25</sup> using LEED, x-ray photoelectron spectroscopy (XPS), and infrared reflection absorption spectroscopy (IRAS) of adsorbed CO. Based on these studies it was concluded that Pd clusters contain primarily (100) and (110) facets at low Pd coverage ( $< 3$  ML) and low surface temperature (300 K), while the (111) facets dominate at high Pd coverage (10–20 ML) and high surface temperature (500 K). The latter was confirmed by the presence of a hexagonal LEED pattern. Recently, Madey<sup>26</sup> examined this system using low-energy ion scattering (LEIS), LEED, and angular-resolved XPS (ARXPS) and found that Pd grows three dimensionally on the  $\text{TiO}_2(110)$  surface at room temperature. Furthermore, it was found that the Pd clusters were encapsulated by  $\text{TiO}_x$  suboxides after annealing to 775–975 K.

## II. EXPERIMENTAL SECTION

The experiments were carried out in an UHV chamber, equipped with a quadrupole mass spectrometer, a UHV-STM (Omicron), and with facilities for LEED and Auger electron spectroscopy (AES). The base pressure was  $< 5 \times 10^{-11}$  Torr. The  $\text{TiO}_2(110)$  sample (Commercial Crystal Laboratories, Inc.) was mounted on the STM sample holder (Ta) using Ta strips. A W-5% Re/W-26% Re thermocouple was glued to the edge of the  $\text{TiO}_2$  crystal using high-temperature ceramic adhesive (AREMCO 571). The thermocouple was used to measure the surface temperature and to calibrate a pyrometer (OMEGA OS3700), which was then used to measure the temperature in subsequent experiments. The  $\text{TiO}_2(110)$  surface was cleaned after cycles of Ar sputtering (1 keV, 8  $\mu\text{A}$ ) and annealing to 700–1000 K. The annealed  $\text{TiO}_2(110)$  surface became deep blue and was sufficiently conductive for STM studies due to the presence of oxygen vacancies in the bulk.

The Pd clusters were prepared by evaporating Pd onto the

$\text{TiO}_2(110)$  surface at 300 K. The source used for Pd deposition was a 0.25 mm Pd wire (99.997%, Johnson Matthey Chemical Limited) wrapped around a tungsten filament and was extensively outgassed prior to use. The pressure during evaporation never exceeded  $2 \times 10^{-10}$  Torr. The flux was calibrated using AES of Pd on the Re(0001) surface and verified using STM. The Pd coverage and flux are given as monolayers (ML) and ML/min, respectively; one ML corresponds to  $1.516 \times 10^{15}$  atoms/cm<sup>2</sup>.

The STM tip was made from a tungsten wire (0.020 in. in diameter, H&R Cross) and prepared by electrolytic etching/polishing.<sup>27</sup> To remove the oxide layer formed on the tip surface during the electrolytic polishing, the tip was etched in HF solution for about 30 s prior to a rapid transfer into the UHV chamber. Before use, the tip was heated briefly to  $\sim 1000$  K.

## III. RESULTS

### A. Clean $\text{TiO}_2(110)$ surface

The morphology of the  $\text{TiO}_2(110)$  surface depends markedly on the sample preparation conditions. Generally, the surface becomes smoother and the terraces wider with each sputter and anneal cycle. This is demonstrated in Fig. 2, which shows two constant current topographic (CCT) STM images of the  $\text{TiO}_2(110)$  surface. The top image was acquired after  $\sim 10$  sputter/anneal cycles (30 min sputtering and 1–5 min annealing between 700 and 1000 K for each cycle) of a freshly polished  $\text{TiO}_2$  sample, while the bottom image was taken subsequent to  $> 100$  such sputter/anneal cycles. 80% of the terraces in the top image have the size  $\sim 200 \times 200 \text{ \AA}^2$ , while 50% of the terraces in the bottom image are  $\sim 1000 \text{ \AA}$  in width. However, in both cases only monatomic steps are observed. It is apparent from Fig. 1 that prolonged sputter/anneal cycles produce a very smooth surface.

The surface morphology also depends markedly on the annealing temperature, which is demonstrated in Figs. 3 and 4. The top image in Fig. 3, acquired after annealing the sample to 1000 K, shows large, flat terraces. After annealing to 1000 K, the sample was heated again to 700, 725, and 800 K for 5 min, respectively, and the resulting morphology studied with STM. These results are shown in the bottom of Fig. 3 (700 K) and in Fig. 4 (top, 725 K and bottom, 800 K). The surface shows a dramatic change after annealing to temperatures as low as 700 K, even though it was preannealed to 1000 K. Stripes, which are only one atomic layer deep, run along the [001] direction on the flat terrace. On the step edge, indentations along the [001] direction are also observed. The stripes also tend to grow next to each other and are separated by a bright, but rather broad row. Increasing the anneal temperature to 725 K leads to a further increase in the density of the stripes as shown in the top image in Fig. 4. However, the surface after annealing to 800 K shows no such stripes. Instead, rectangular depressions along the [001] direction and small protrusions with monatomic height are observed. The images acquired after annealing to 900 K (not shown) are virtually identical to those obtained directly after annealing to 1000 K.

Figure 5 provides a small area STM image of the surface annealed to 725 K, and shows atomic resolution of both un-

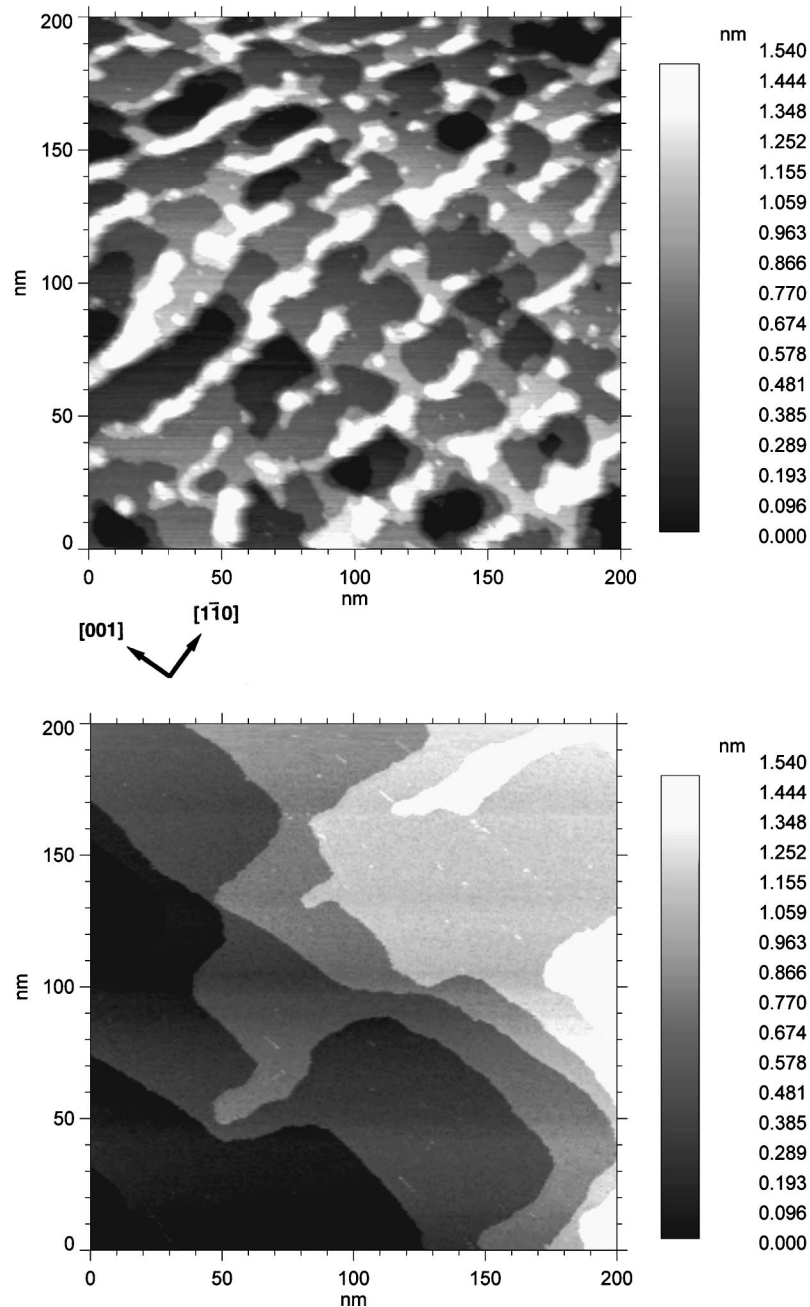


FIG. 2. CCT STM images of the  $\text{TiO}_2(110)$  surface acquired after about 10 sputtering/annealing cycles (30 min sputtering and 1–5 min annealing between 700 and 1000 K) (top image) and over 100 such cycles (bottom images). The sample bias and feedback current are 2 V and 0.5 nA, respectively.

reconstructed and reconstructed areas. On the bottom-left and top-right side of the image, the distance between the individual atom rows is  $\sim 6.5 \text{ \AA}$ , corresponding to the length of the unit cell along the  $[1\bar{1}0]$  direction for the unreconstructed  $(1 \times 1)$   $\text{TiO}_2(110)$  face. The atom rows in the center of the image are much broader than the atom rows in the  $(1 \times 1)$  areas; the smallest distance between these broad atom rows is  $\sim 13 \text{ \AA}$ , twice that of the unit cell along the  $[1\bar{1}0]$  direction. The broad rows were occasionally resolved into two separate, narrow rows and were always terminated by a bright protrusion at the end of the row. Both the shape and periodicity of this structure are in good agreement with the  $(1 \times 2)$  reconstruction of the  $\text{TiO}_2(110)$  surface observed

previously after annealing the sample to  $> 1200 \text{ K}$ .<sup>11–16</sup> This behavior was also observed in the present work. Altogether, these results indicate two temperature ranges for preparing the  $(1 \times 2)$  reconstructed  $\text{TiO}_2(110)$  surface: 700–800 K and higher than 1200 K. These two temperature ranges are apparently separated by a temperature region where the  $(1 \times 1)$  unreconstructed  $\text{TiO}_2(110)$  surface is the most stable phase. From Fig. 5, it is apparent that the layer under the  $(1 \times 2)$  reconstructed area shows a  $(1 \times 1)$  structure, indicating that the reconstruction is only one atom layer deep.

It is also noteworthy that the  $(1 \times 2)$  reconstructed surface produced between 700 and 800 K reversibly converts to the  $(1 \times 1)$  unreconstructed surface. This conversion seems to

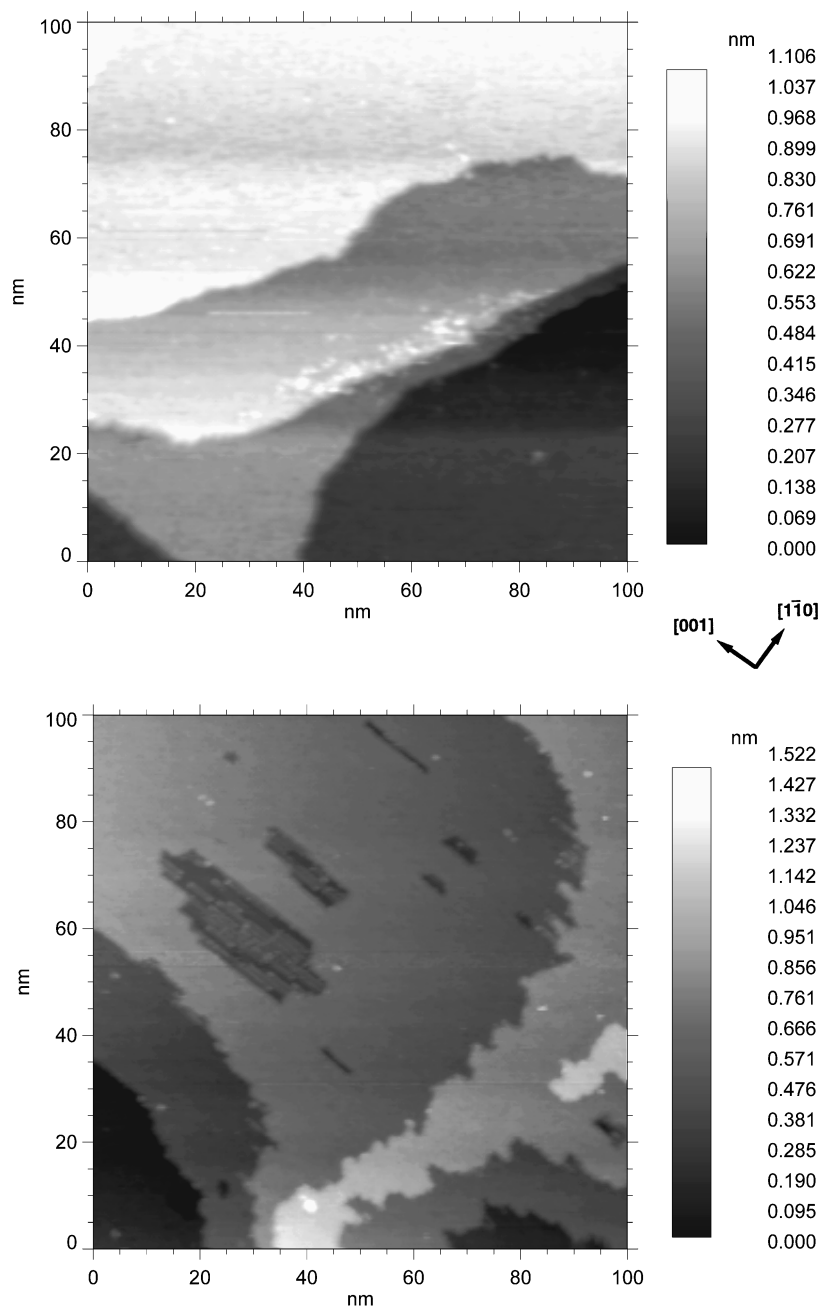


FIG. 3. CCT STM images of the  $\text{TiO}_2(110)$  surface after annealing to 1000 (top) and subsequently annealing to 700 K (bottom).

occur by the disappearance of the reconstructed layer, probably through oxygen desorption into the gas phase and/or via Ti diffusion into the bulk. This is indicated by the appearance of the rectangular depression and isolated bright spots after annealing to 850 K, features apparently left behind by the  $(1 \times 2)$  reconstructed layer.

A high-resolution STM image was also obtained for the  $(1 \times 1)$   $\text{TiO}_2(110)$  surface after annealing to 1000 K (Fig. 6). The individual atoms are clearly resolved in this image. After a scanner calibration using a graphite sample, the distance between adjacent atoms along the  $[001]$  and  $[1\bar{1}0]$  directions were measured to be 3 and 6.5 Å, respectively, in very good agreement with the unit cell of the  $(1 \times 1)$   $\text{TiO}_2(110)$  sur-

face, shown schematically in Fig. 1. It is also noteworthy that this image shows a very large corrugation of  $\sim 2$  Å along the  $[1\bar{1}0]$  direction and  $\sim 1$  Å along the  $[001]$  direction, as indicated by the line profile in Fig. 6. Since the image was acquired at a rather small sample bias of 0.16 V and feedback current of 2.5 nA, the STM tip is likely in the near contact scanning mode. The close proximity of the tip to the surface can strongly perturb the surface electronic structure and induce a tip-induced localized state (TILS).<sup>28</sup> It has been demonstrated that the corrugation in the STM image can be significantly enhanced by the presence of TILS.<sup>28</sup> An alternative explanation, although less likely, is that the close proximity of the tip to the surface induces a mechanical de-

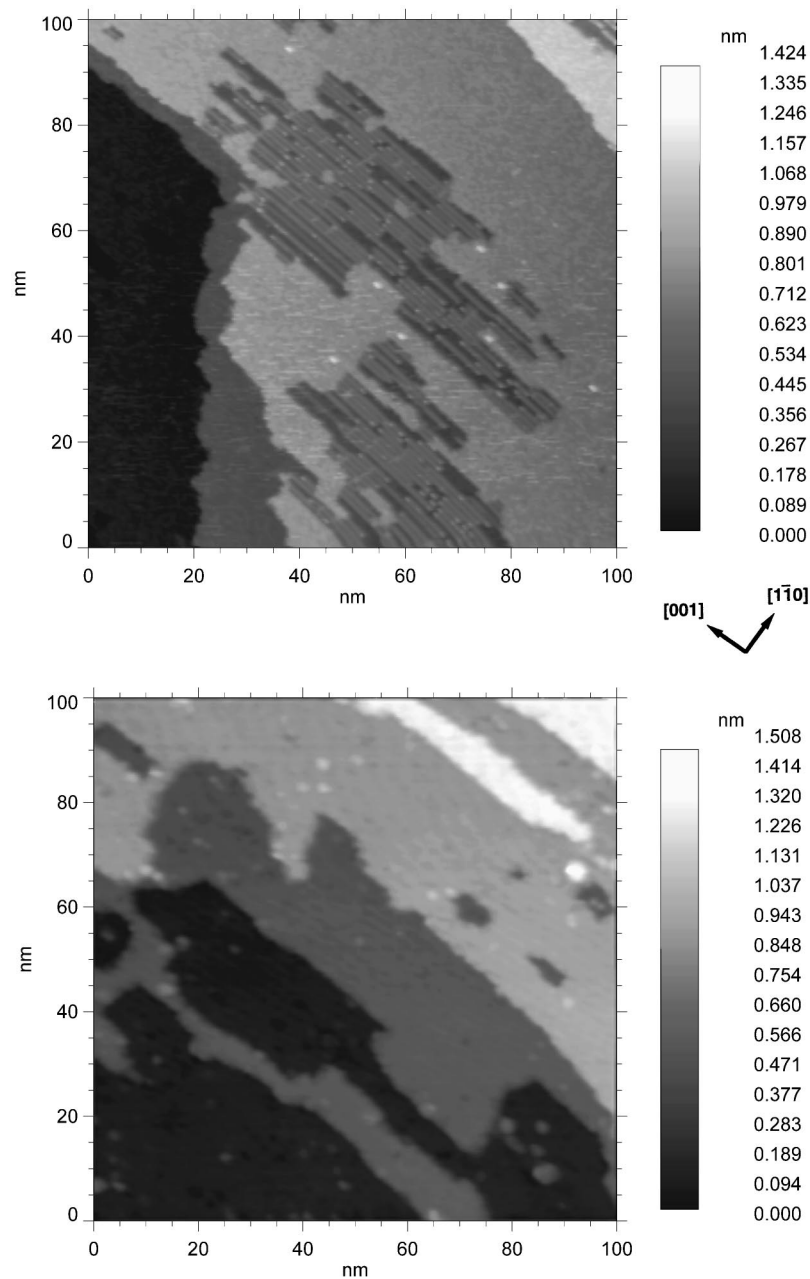


FIG. 4. CCT STM images of the  $\text{TiO}_2(110)$  surface after annealing to 1000 K and subsequently annealing to 725 (top) and 800 K (bottom).

formation of the surface, resulting in a large corrugation in the STM image. Such effects have been observed for relatively soft materials such as graphite.<sup>28</sup>

Three irregular atoms were also observed in this image: one located between the third and fourth rows from the top, one between the fourth and fifth rows from the top, and one between the fourth and fifth rows from the bottom. It should be noted that all three of these irregular atoms are located at the same site, somewhere between the bridging site and the fourfold-hollow site. Assuming that the bright spots arise from Ti cations, these data are consistent with the presence of oxygen vacancies on the surface. A single oxygen atom vacancy would expose two adjacent Ti cations

equally (as shown in Fig. 1), which would lead to a structure inconsistent with our STM images. However, an oxygen vacancy with two missing adjacent oxygen atoms would expose the Ti cation in the center more so than the two adjacent Ti cations. The Ti cation in the center, which is only fourfold coordinated, would then relax from the bridge site to the fourfold site, assuming a fivefold-coordination position. However a repulsive interaction with the adjacent Ti cations would prevent complete relaxation. In balancing these two interactions, the Ti cation should relax into a site between the twofold-bridge and fourfold-hollow site, consistent with the STM image. This result also implies that the oxygen vacancy is created by removing two adjacent oxygen atoms, most

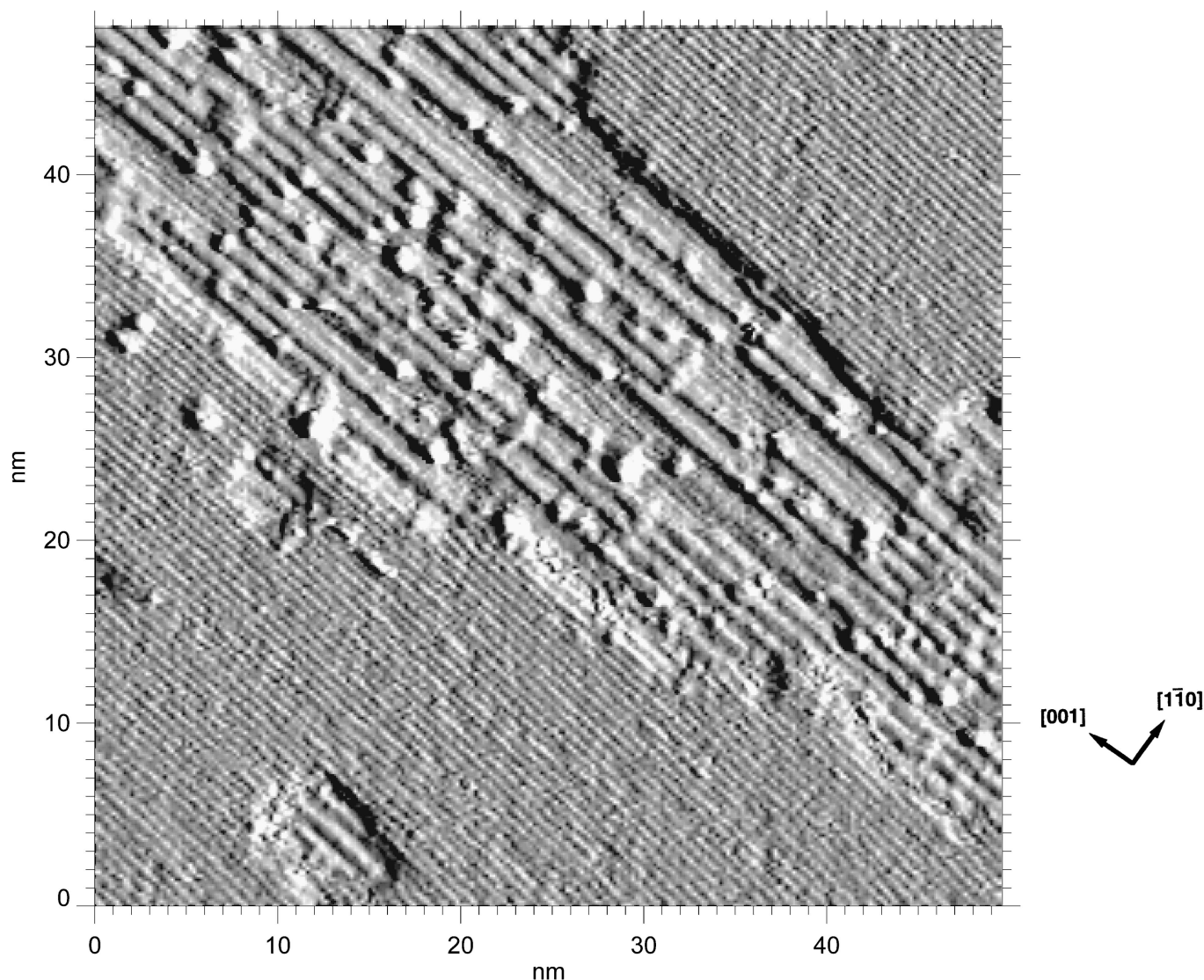


FIG. 5. A expanded view of an STM image of the  $\text{TiO}_2(110)$  surface after annealing to 1000 K and subsequently annealing to 725 K.

likely via recombinative desorption into the gas phase. An alternative explanation, although less likely, is that these defects arise from surface contamination.

The high-resolution STM images depend markedly on the nature of the STM tip. Occasionally, very different images were obtained after an apparent tip change during the scan. This behavior is likely related to tip modification by the surface, probably through accumulation by the tip of a surface atom. Figure 7 shows two images that were observed repeatedly on a  $(1 \times 1)$  surface after a tip modification of this kind. The top image, observed frequently at a sample bias between 0.5 and 1 V and found to be stable over several scans, has ridges running along the  $[001]$  direction. The adjacent atom rows exhibit varying degrees of brightness and are separated by  $\sim 3.3 \text{ \AA}$ . It should also be noted that the individual atoms are located along a line running in the  $[\bar{1}10]$  direction. Referring to the schematic drawing for the  $\text{TiO}_2(110)$  surface in Fig. 1, these results indicate that both Ti and O ions are being imaged in this STM scan.

The bottom image in Fig. 7 shows an example where the STM image was modified during the scan. The image was acquired with the STM tip scanning from left to right and

moving from bottom to top on a  $(1 \times 1)$   $\text{TiO}_2(110)$  surface covered with 0.02 ML Pd. At the bottom of the image, the typical ridge structure is apparent along the  $[001]$  direction; the ridges are broad and rather poorly resolved. At  $\sim 1.2 \text{ nm}$  from the bottom, as indicated by the arrow 1, a clear change in the image is apparent. Instead of the broad ridges, well-resolved atom rows are observed. It is noteworthy that the atoms are located between the broad ridges found at the bottom of the image. At the middle of the scan, indicated by the arrow 2, a second change in the image is seen. Instead of the well-resolved atom rows, broad ridges are once again observed and are located between the well-resolved atom rows. The distance between the adjacent rows is  $\sim 6.5 \text{ \AA}$  in both cases. These results demonstrate that a change of the imaged ions has occurred during the scan and indicate that both Ti and O ions can be imaged depending upon the nature of the STM tip.

#### B. Pd supported on $\text{TiO}_2(110)$

Figure 8 shows two CCT STM images of Pd on two different  $\text{TiO}_2(110)$  surfaces. The  $\text{TiO}_2(110)$  substrate in the top

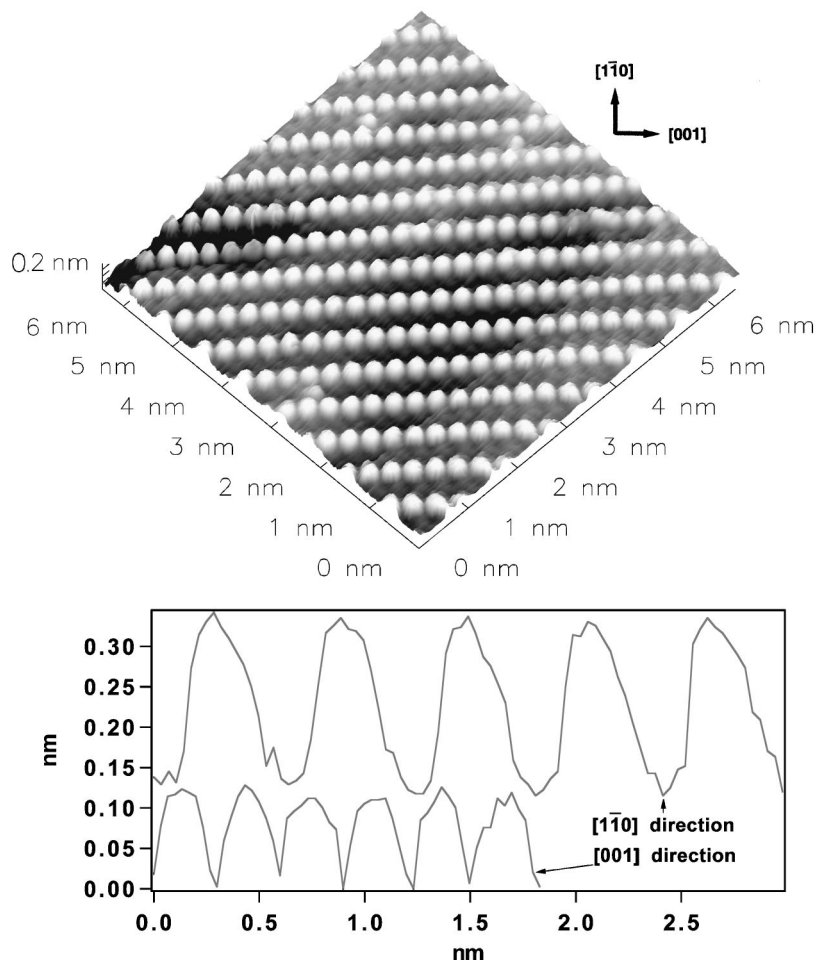


FIG. 6. High-resolution STM image of the TiO<sub>2</sub>(110) surface (top) and two line profiles along the  $[1\bar{1}0]$  and  $[001]$  directions. The sample bias and feedback current were 0.16 V and 2.5 nA, respectively.

image was subjected to only a few sputter/anneal cycles and consequently has a much higher density of steps than the substrate in the bottom image. The latter was cleaned by  $>100$  sputter/anneal cycles and shows much larger, flatter terraces. The Pd coverages and dose fluxes were 0.25 ML and 0.5 ML/min for the top image, and 0.13 ML and 0.1 ML/min for the bottom image, respectively. In both cases, hemispherical clusters with a very narrow size distribution were observed. In addition, there is clear preferential nucleation of clusters on the step edges for both surfaces; however, clusters on the flat terrace are also observed, indicating the presence of nucleating sites there as well. It should be noted that the top image has a smaller average cluster size and higher cluster density compared to the bottom image. The larger cluster sizes in the bottom image compared to the top image are especially remarkable, since the bottom image corresponds to a lower Pd coverage. Two factors contribute to this difference. First, the top surface contains a higher density of steps and therefore has more nucleation sites than the bottom surface to stabilize cluster formation. Second, the higher Pd flux used to prepare the surface for the top image (0.5 versus 0.1 ML/min for the bottom image) should also result in a larger number of nuclei compared to that of the bottom image. Since there is no clear difference in the size between the clusters at the step edge and the clusters on the terrace in both images, we infer that the difference in flux

was the main reason for the observed cluster size differences in the two images. This similarity in size distributions suggests competition between nucleation of sites and growth of the clusters. Furthermore, the higher flux apparently leads to a narrower cluster size distribution compared to the lower flux.

In Figs. 9 and 10, an expanded view of four different Pd coverages is shown for similar TiO<sub>2</sub>(110) substrates. The Pd flux was 0.1 ML/min and the coverages were 0.012 ML for Fig. 9(a) 0.13 ML for Fig. 9(b) 0.22 ML for Fig. 10(a), and 0.43 ML for Fig. 10(b). At a Pd coverage of 0.012 ML, 80% of the clusters are  $2.5 \pm 0.5$  Å high, corresponding to a single Pd layer, and have a diameter of  $20 \pm 2$  Å. Clusters having a height of 6 Å and a diameter of about 30 Å were also observed. These results indicate a bimodal distribution of the cluster sizes at this Pd coverage, correlating with a transition from two-dimensional (2D) to 3D growth of Pd. The transition from 2D to 3D growth at such low Pd coverages (0.012 ML) demonstrates that Pd grows in a Volmer-Weber mode on this surface.

With increasing Pd coverages, the cluster size increases dramatically, while the increase in the cluster density is rather small. This is more clearly seen in Fig. 11, in which the cluster density and size are plotted versus the Pd coverage. A very rapid increase in the cluster density is seen initially upon deposition of 0.012 ML Pd. With a further in-

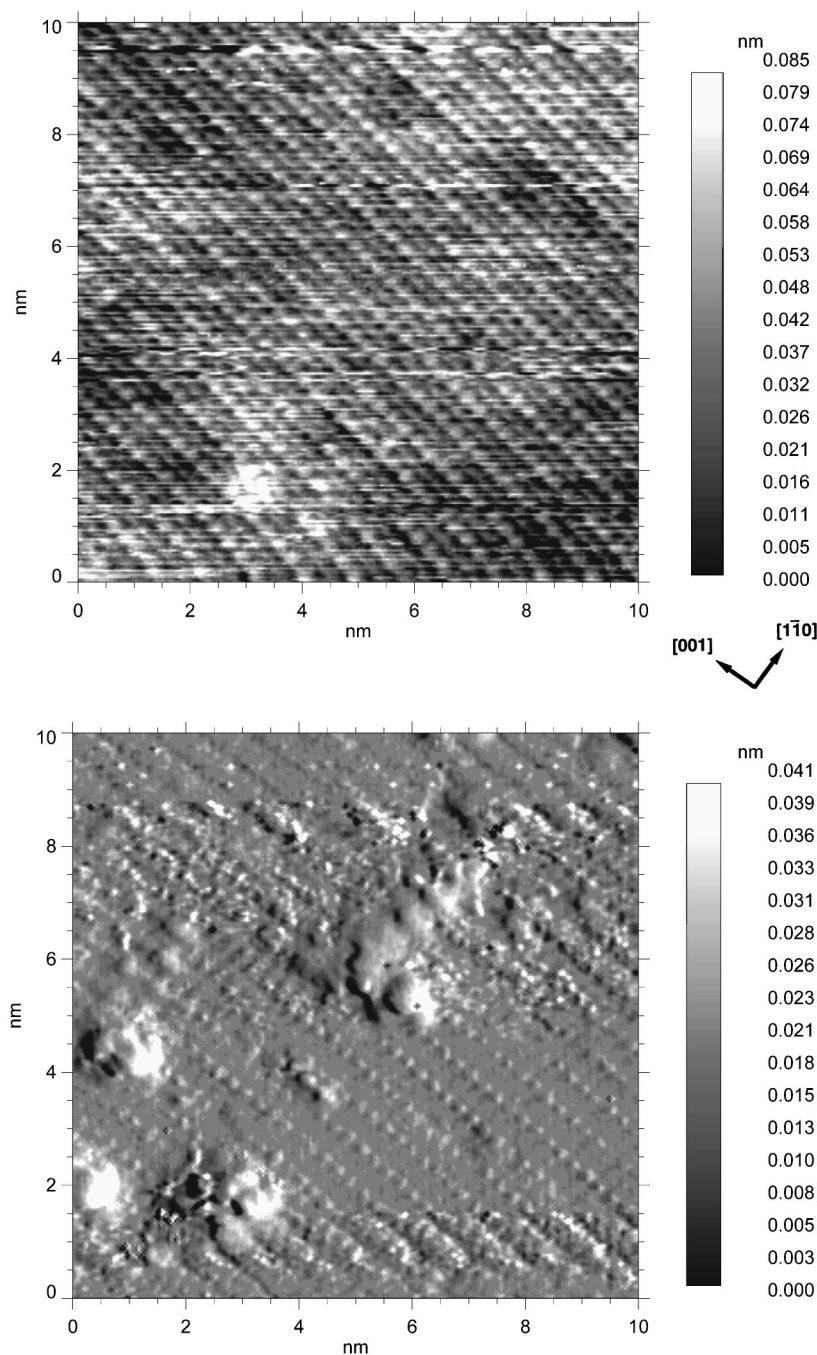


FIG. 7. CCT STM images of the  $\text{TiO}_2(100)$  surface (top, 0.5 V and 1 nA) and 0.02 ML Pd on the  $\text{TiO}_2(110)$  surface (bottom, 0.5 V and 1 nA).

crease in the Pd coverage from 0.012 to 0.13 ML, the cluster density increases only by  $\sim 25\%$  and increases yet again by  $\sim 25\%$  from 0.13 ML to 0.22 ML Pd. At higher Pd coverages, the cluster density begins to decline likely due to cluster coalescence. These results indicate that  $\sim 65\%$  of the nucleation sites are formed at a Pd coverage as low as 0.012 ML and the nucleation process is essentially complete at a Pd coverage of  $\sim 0.2$  ML. In contrast, the cluster size increases continuously with increasing Pd coverage, with an enhanced rate of increase at the higher Pd coverages. These results demonstrate that nucleation dominates at small Pd coverages (0–0.2 ML), while the cluster growth dominates at higher Pd coverages ( $>0.1$  ML).

Due to the large surface corrugation associated with large Pd clusters at high Pd coverages, stable images such as those of Fig. 10 can only be obtained at rather high sample bias voltages (4 V). Such high voltages keep the tip sufficiently far from the surface to avoid a tip crash during the scan. At small Pd coverages ( $<0.2$  ML), the Pd clusters are rather sensitive to the tip. A large tip-sample distance is mandatory during the STM experiments to avoid tip-induced modification of the cluster.

It is noteworthy that atomic resolution was achieved on the  $\text{TiO}_2(110)$  substrate in all four images of Figs. 9 and 10. The individual atom rows, spaced  $6.5 \text{ \AA}$  from each other, run along the [001] direction. Close inspection of the individual

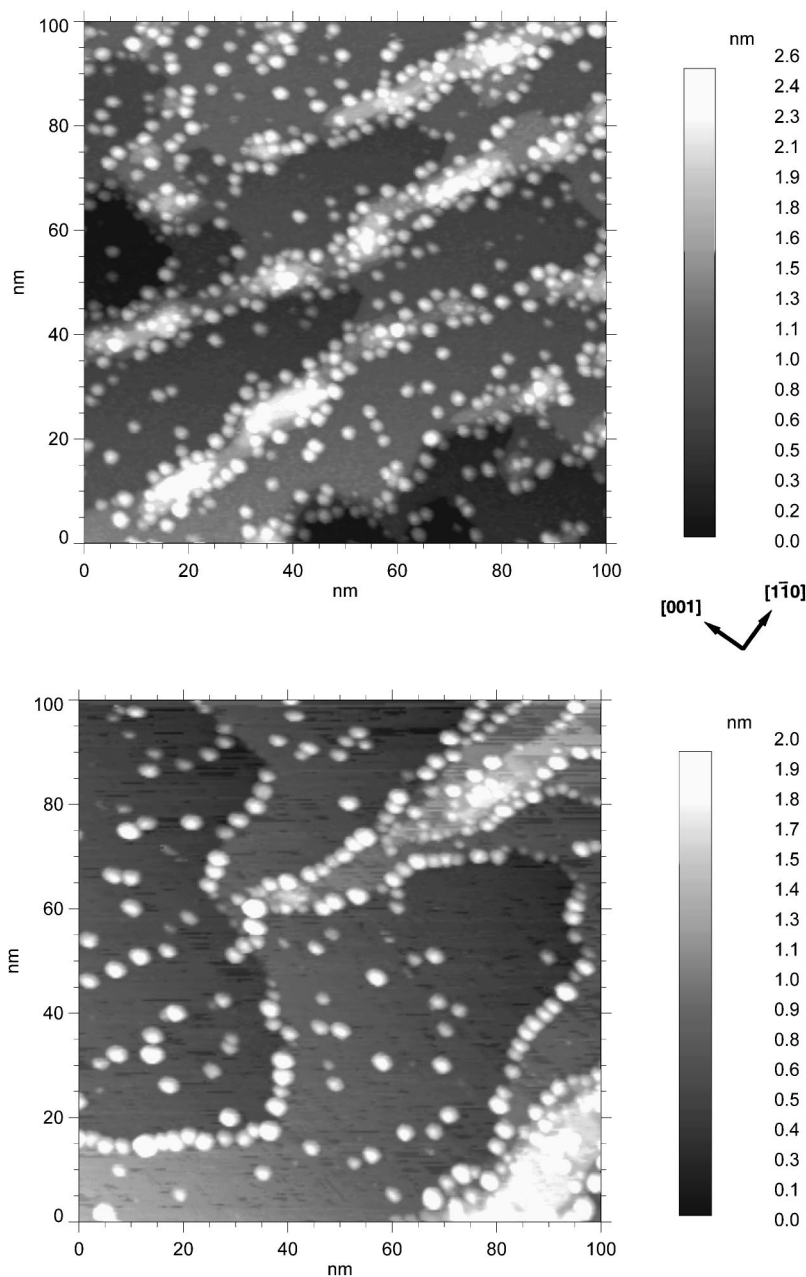


FIG. 8. CCT STM images of 0.25 ML Pd (top) and 0.13 ML Pd (bottom) on the  $\text{TiO}_2(110)$  surface. The Pd dosing rate was 0.5 ML/min for the top image and 0.13 ML/min for the bottom image.

3D Pd clusters shows either no atomic resolution or a disordered structure; Fig. 12 shows such an image for a disordered Pd cluster. However, atomic resolution with ordered structures was occasionally achieved for the 2D Pd clusters. Figure 13 shows two STM images of  $\sim 0.02$  ML Pd on the  $\text{TiO}_2(110)$  surface, which exhibit areas with predominantly 2D Pd clusters. The Pd flux used to prepare this sample was 0.5 ML/min, a flux sufficiently high to yield more highly dispersed (smaller) Pd clusters. As the top image shows, the small Pd clusters are elongated along the  $[001]$  direction. Most of the clusters are only one atom in height and are located directly on top of the bright rows of the substrate atoms. This can be more clearly seen in the bottom image, which shows an expanded view. In this image, three dimers are observed aligned along the  $[001]$  direction; the distance

between the two atoms is  $\sim 3.5 \text{ \AA}$ . A tetramer, with a similar Pd-Pd distance along the  $[001]$  direction as the dimer, is also seen in this image. The Pd-Pd distance along the  $[110]$  direction is  $\sim 6.5 \text{ \AA}$ , corresponding to the lattice constant of the  $\text{TiO}_2(110)$  substrate in the  $[110]$  direction, indicating pseudomorphic growth of Pd. Since the adjacent Pd-Pd distance on the more open Pd(110) surface is  $2.75 \text{ \AA}$  along the  $[110]$  direction and  $3.89 \text{ \AA}$  along the  $[100]$  direction, the Pd-Pd bond in the two-dimensional cluster on  $\text{TiO}_2(110)$  is significantly stretched and likely rather weak. Therefore, the structure of the 2D Pd cluster is primarily determined by the Pd-substrate interaction. However, it is unlikely that the loss of the Pd-Pd bond energy can be fully compensated by the formation of a Pd-substrate bond; that is, the tetramer is likely metastable thermodynamically.

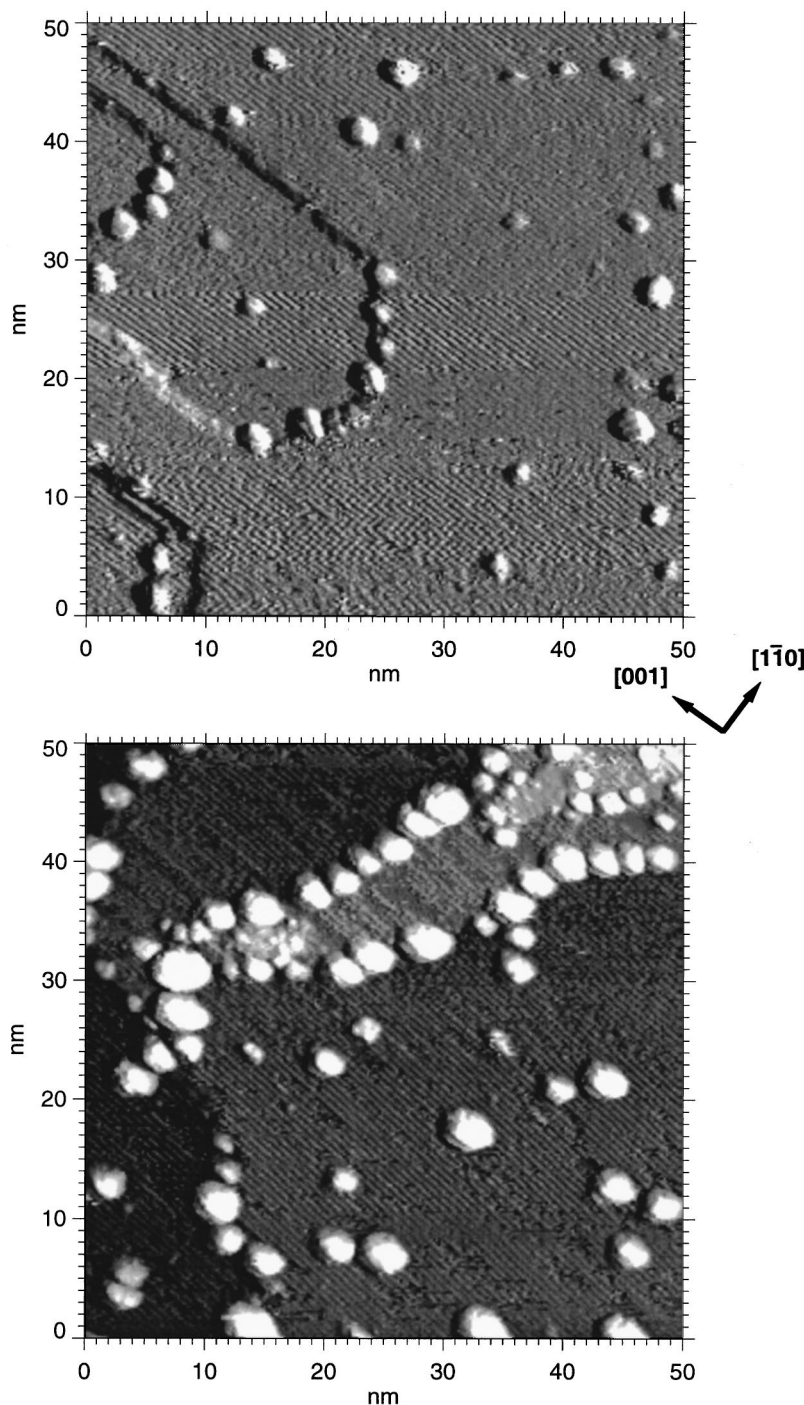


FIG. 9. CCT STM images of 0.012 ML Pd (top) and 0.13 ML Pd (bottom) on the  $\text{TiO}_2(110)$  surface. The Pd dose flux was 0.1 ML/min. The sample bias and feedback current were 2 V and 1.7 nA, respectively.

Since the bright ridges of the substrate in Fig. 13 arise from the fivefold-coordinated Ti rows, it can be concluded from this image that Pd atoms adsorb initially on the fivefold-coordinated Ti cations between two bridging oxygen rows, likely between two adjacent Ti cations. It also should be noted that no isolated Pd atoms were ever observed, suggesting that the dimer is the smallest stable nuclei.

As demonstrated previously,<sup>29-31</sup> STM experiments can lead to significant overestimation of cluster sizes due to the convolution of the STM tip and the fact that the density of states is the quantity actually measured. Therefore, the apparent cluster size measured by STM can be significantly

larger than the actual cluster size. Since atomic resolution has been routinely achieved on the  $\text{TiO}_2(110)$  substrate in our experiments and even occasionally on the Pd clusters, the broadening due to convolution of the STM tip should be rather small and more likely dominated by electronic effects. To evaluate the electronic effect on the measured cluster size, we have compared the cluster size measured in STM with the average cluster size calculated by assuming the same density of the Pd clusters as in bulk Pd and using the known Pd coverage and cluster density. For a Pd coverage of 0.25 ML, this calculation results in a cluster size estimate of 341 atoms/cluster. This estimate is very close to a cluster

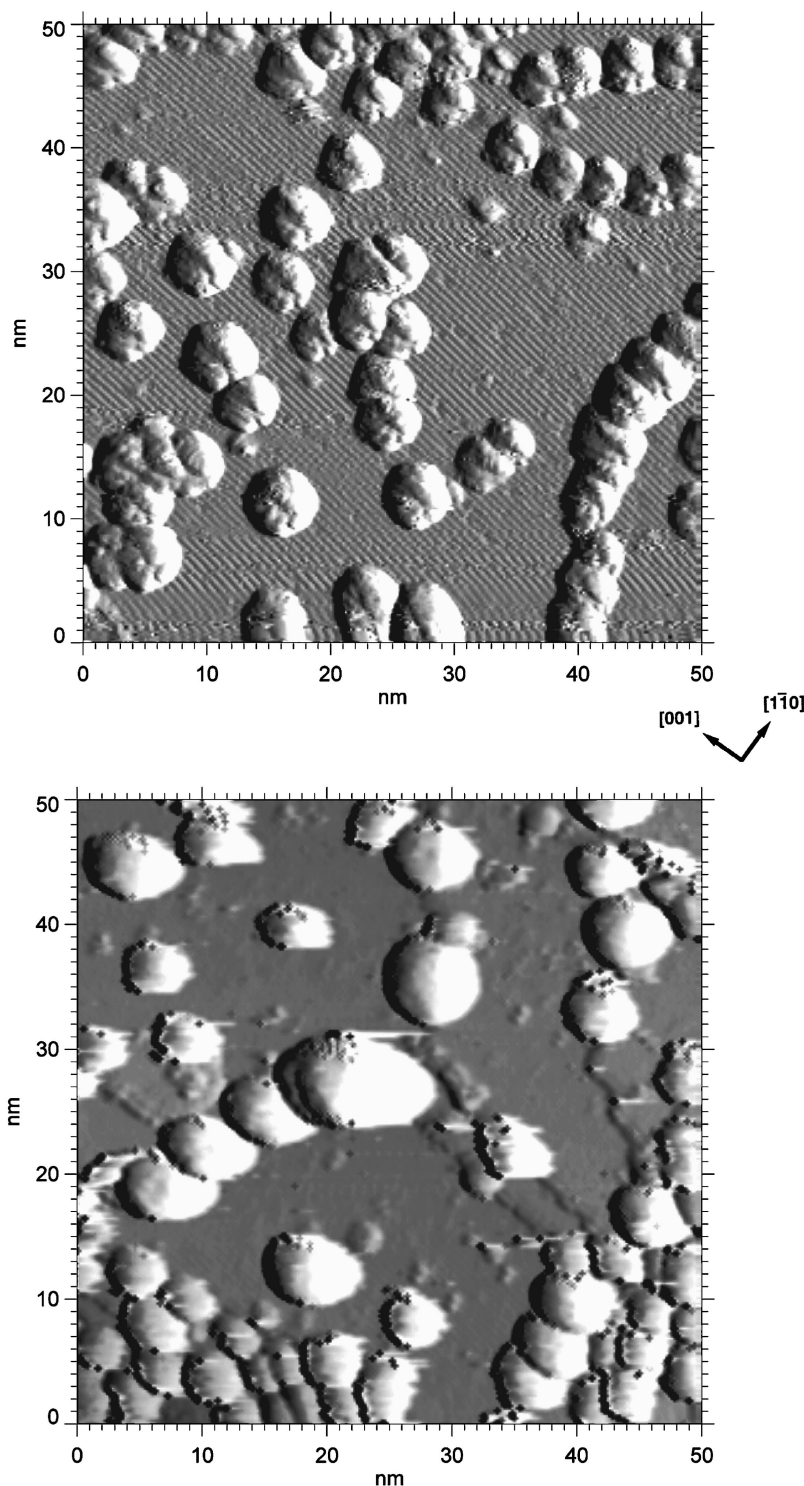


FIG. 10. CCT STM images of 0.22 ML Pd (top) and 0.43 ML Pd (bottom) on the TiO<sub>2</sub>(110) surface. The Pd dose flux was 0.1 ML/min. The sample bias and feedback current were 4 V and 2 nA, respectively.

size of 349 atom/cluster measured in the STM image; the small difference is well within the experimental error. These results clearly indicate that the Pd cluster size measured under our experimental conditions does indeed represent the actual cluster size and that broadening due to electronic effects is negligible.

One of the important questions regarding the interaction of supported metal clusters with adsorbed molecules is how the structure of the metal cluster responds to the adsorption.

It has been assumed and observed that adsorbates can induce a reconstruction of the substrate.<sup>32-34</sup> To study the effect of CO adsorption on the structure of supported Pd clusters, CO was leaked into the chamber during the STM imaging. No significant changes of the Pd cluster size and shape were found at a CO pressure up to  $1 \times 10^{-5}$  Torr and CO exposure times up to several hours. The influence of background CO on the Pd nucleation and growth on the TiO<sub>2</sub>(110) surface was also studied. Figure 14 compares the STM image of 0.22

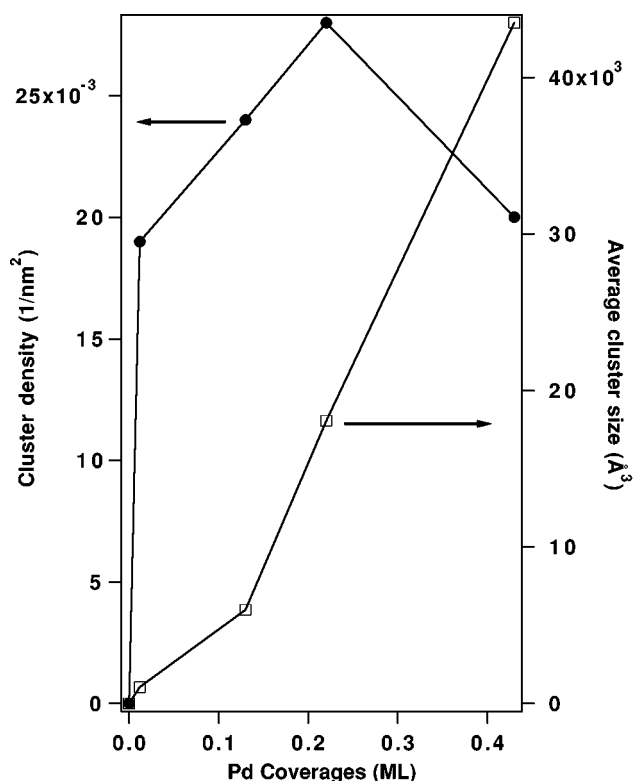


FIG. 11. Plot of the cluster density and size vs the Pd coverage.

ML Pd deposited onto  $\text{TiO}_2(110)$  in vacuum with the image acquired after deposition of the same quantity of Pd under  $1 \times 10^{-6}$  Torr CO. The surface prepared by depositing Pd with CO in the background shows a larger cluster size and

lower cluster density than the surface prepared by depositing Pd without CO. The average cluster density and size are  $0.0096/\text{nm}^2$  and  $57 \times 25 \text{ \AA}^2$  (diameter  $\times$  height) for Pd deposition with  $1 \times 10^{-6}$  Torr background CO and  $0.028/\text{nm}^2$  and  $54 \times 14 \text{ \AA}^2$  for Pd deposition without CO. The presence of CO induces a marked decrease of the cluster density and an increase in cluster size, particularly for the height of the cluster.

It is also noteworthy that some of the clusters in Fig. 14 have a rectangular shape and are aligned along the  $[001]$  direction of the  $\text{TiO}_2(110)$  substrate. The shape and orientation of these clusters indicate the formation of either Pd(110) or Pd(100) microcrystals on the  $\text{TiO}_2(110)$  surface. The formation of microcrystals can be more clearly seen at high Pd coverages and high annealing temperatures. Figure 15 shows a STM image acquired after exposure of the  $\text{TiO}_2(110)$  surface to 1.1 ML Pd and a subsequent anneal to 1000 K. In addition to several rectangular-shaped clusters, most of the clusters have a hexagonal shape and are aligned with two of the six edges along the  $[001]$  direction. This indicates the formation of Pd(111) microcrystals, which apparently dominate the structure of the clusters at this coverage and annealing temperature. It should also be noted that the top surface of the cluster is rather smooth. A typical line profile over one of the cluster in Fig. 15 shows that the top surface is atomically flat over  $\sim 100 \text{ \AA}$ .

The electronic structure of the Pd cluster was also studied using scanning tunneling spectroscopy (STS). The STS measurements were carried out during the topographic scan by stopping the scan at selected pixels, interrupting the STM feedback loop, then sweeping the bias voltage through the region of interest. The topographic scan can be used to cor-

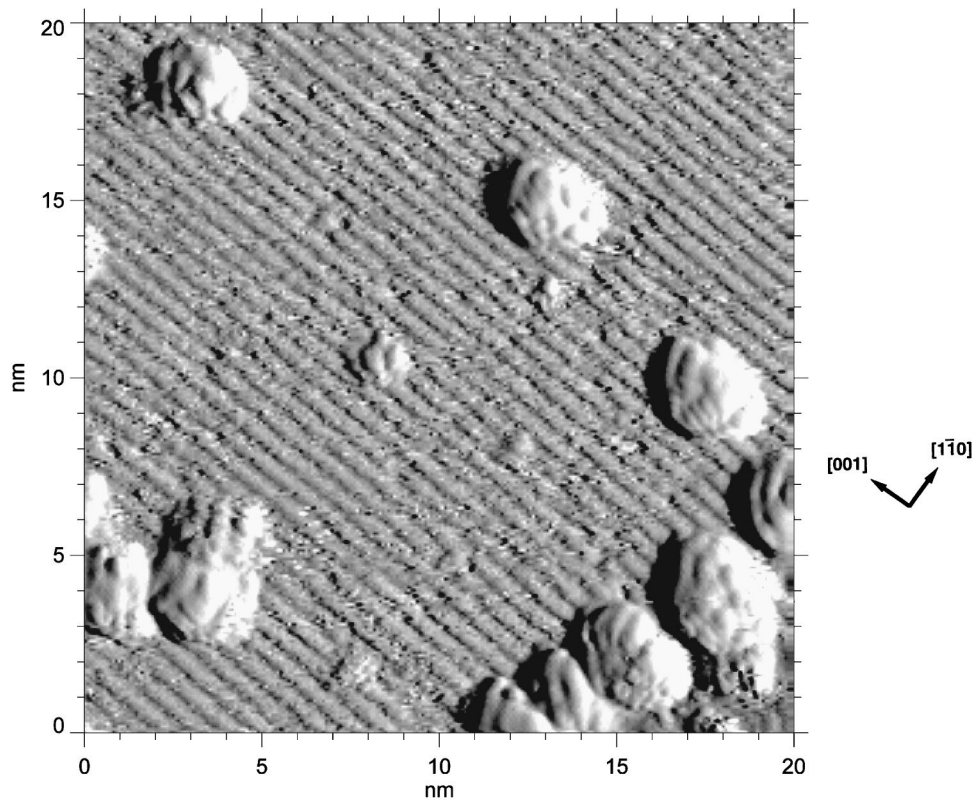


FIG. 12. CCT STM image of 0.25 ML Pd on the  $\text{TiO}_2(110)$  surface (1.5 V, 0.5 nA).

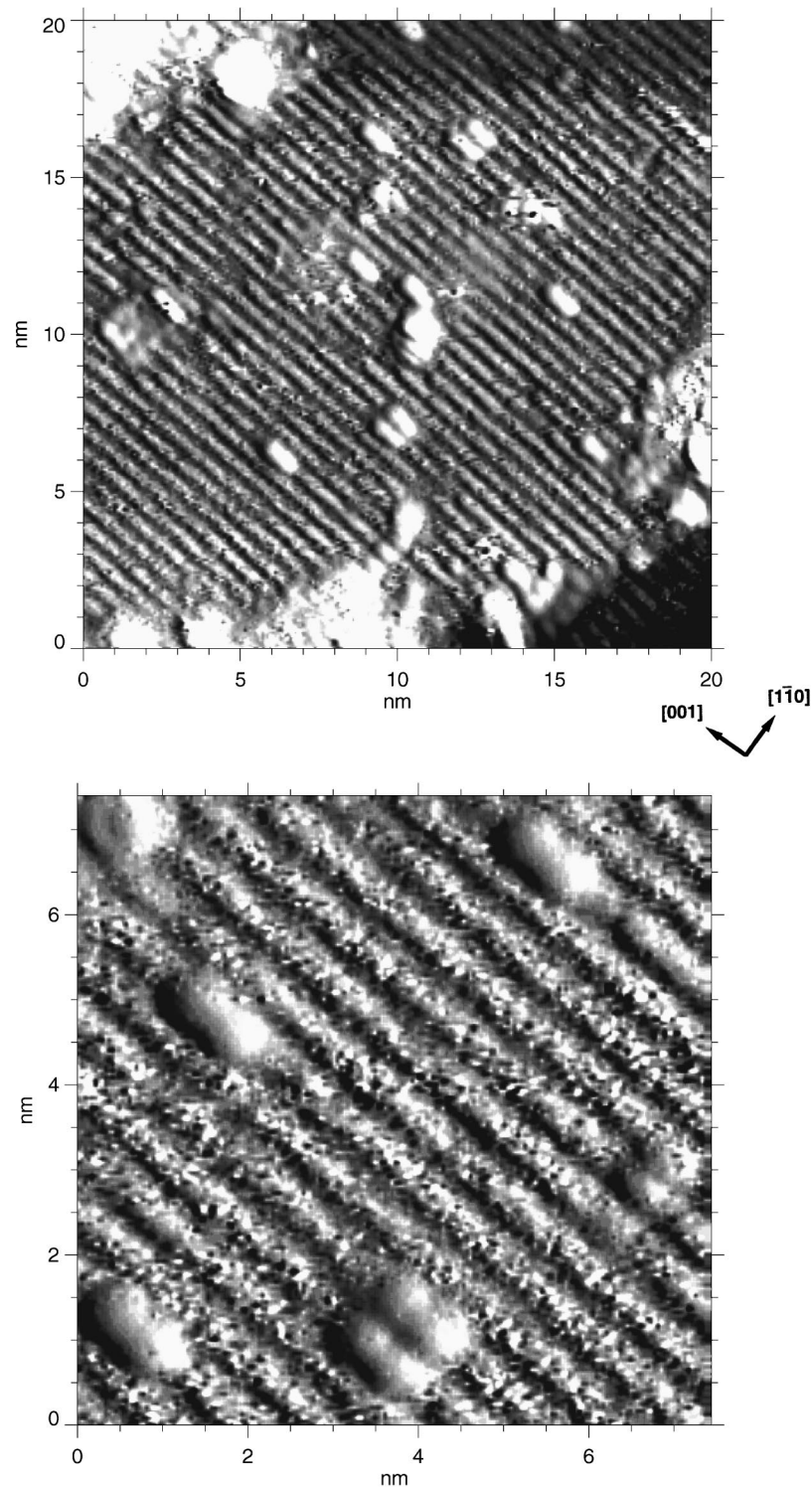


FIG. 13. CCT STM images of 0.02 ML Pd on the  $\text{TiO}_2(110)$  surface (2 V, 1 nA). The Pd deposition rate was 0.5 ML/min.

relate the STS curve with a particular geometric feature and, as well, provide a check for tip stability during the measurements. Figure 16 provides a series of expanded views of several STS curves with the inset showing the full spectra, characteristic of different Pd coverages. The STS data were acquired on individual clusters, whose size are indicated in the figures along with the Pd coverage.

The  $\text{TiO}_2(110)$  substrate displays a band gap of only 0.8 eV, however, the tunneling current at a bias of  $-0.5$  to

$-1.8$  V is rather low, suggesting that the primary contributors to the tunneling current are minority defects. The extensive heating and sputtering onto the  $\text{TiO}_2$  sample has created subsurface defects and therefore states in the band gap. Depending on the sample bias and feedback current, one can have very different sensitivities to the defect states. In our experiments, a rather low bias and high feedback current were used and therefore the defect states were also detected. As discussed above, the Pd clusters exhibit a bimodal size

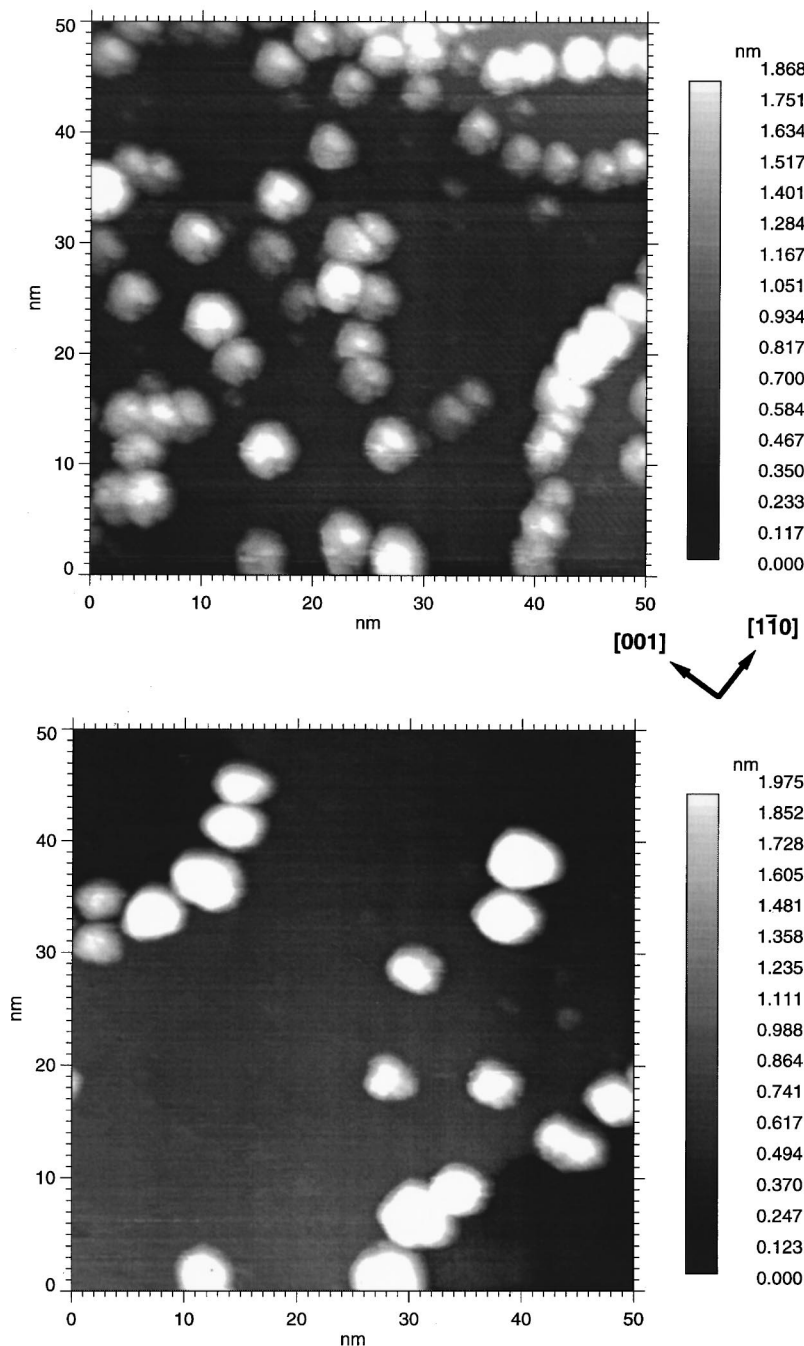


FIG. 14. CCT STM images of 0.22 ML Pd deposited with  $1 \times 10^{-6}$  Torr background CO (bottom) and without background CO (top) onto the  $\text{TiO}_2(110)$  surface.

distribution at 0.012 ML, corresponding to the transition from 2D to 3D growth of Pd on the  $\text{TiO}_2(110)$  surface. The STS curves were obtained for both 2D and 3D clusters. The 2D cluster, which has a diameter of  $\sim 18 \text{ \AA}$  and a height of  $3 \text{ \AA}$ , shows a band gap of  $\sim 2 \text{ V}$  in the STS curve; the Fermi level is strongly pinned towards the conduction band, very similar to that of the  $\text{TiO}_2(110)$  substrate. Similar  $I$ - $V$  curves have been observed for dimers and tetramers and are very characteristic of the 2D clusters. It is also noteworthy that an increase in the cluster size, although very limited for the 2D clusters, does not alter the  $I$ - $V$  curve significantly. These results indicate a rather weak interaction between adjacent Pd atoms in the 2D cluster, consistent with the topo-

graphic images, which show a significantly stretched Pd-Pd bond. That is, the Pd-substrate interaction dominates the geometric as well as the electronic structure of the 2D Pd cluster. As a consequence of the weak Pd-Pd interaction, the 2D cluster remains nonmetallic. On the other hand, the 3D cluster at the same Pd coverage, which is  $22 \text{ \AA}$  in diameter and  $6 \text{ \AA}$  in height and is only slightly larger than the 2D cluster, shows a rather different  $I$ - $V$  curve. Although it still exhibits a band gap of  $0.8 \text{ V}$ , the magnitude is much smaller than that for the 2D cluster. Increasing the cluster size to  $28 \times 9 \text{ \AA}^2$  at a Pd coverage of 0.13 ML leads to a further reduction in the band gap to  $0.1 \text{ V}$ . For a cluster size of  $43 \times 13 \text{ \AA}^2$  at 0.22 ML Pd, the  $I$ - $V$  curve shows a nonzero tunneling current at

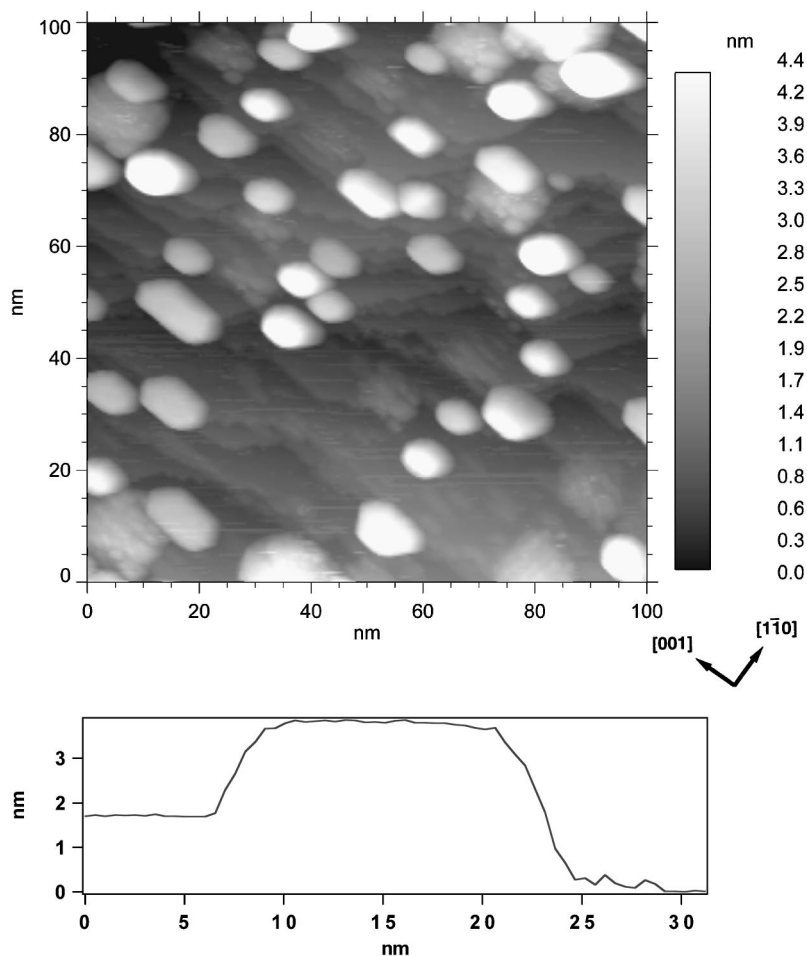


FIG. 15. CCT STM image acquired after annealing a 1.1 ML Pd covered  $\text{TiO}_2(110)$  surface to 1000 K. The line profile over one of the hexagonal cluster is also shown.

$0^+$  and  $0^-$  bias voltage, indicating the onset of metallic behavior. Increasing the cluster size still further causes essentially no change in the resulting  $I$ - $V$  curve. Certainly the cluster can have a smaller band gap than the substrate. Whether one can see it or not in the STM measurements depends only on the rate how fast the electron on the cluster can be dissipated into the substrate. Apparently, the intimate contact of the Pd cluster with the  $\text{TiO}_2$  substrate allows the electron to be transferred away fast enough for measurements.

To eliminate possible substrate effects, STS spectra were acquired for clusters with varying size on the same surface. These data are presented in Fig. 17 with the corresponding topographic scan. To study the effect on the STS measurements of distance between the tip and sample, the STS spectra were acquired at a sample bias of 2 V and six different feedback currents between 1.7 and 6 nA. Virtually identical  $I$ - $V$  curves were obtained after normalizing the individual spectra against the feedback current. (The average  $I$ - $V$  curves over these six measurements are shown in Fig. 17.) For comparison, the  $I$ - $V$  curve for the clean  $\text{TiO}_2(110)$  substrate is also provided. As the topographic image shows, the cluster size increases gradually from  $24 \times 6 \text{ \AA}^2$  for cluster 1 to  $41 \times 15 \text{ \AA}^2$  for cluster 6. The STS curves for clusters 1 and 2 show a rather large band gap of about 0.8 V about the

Fermi level, characteristic of a nonmetallic phase. Cluster 3, which is  $28 \text{ \AA}$  in diameter and  $9 \text{ \AA}$  in height and contains roughly 215 atoms, exhibits a band gap of  $\sim 0.1 \text{ V}$ . The STS curves for clusters 4–6 show a nonzero tunneling at  $0^+$  and  $0^-$ , indicating the metallic nature of these clusters. It should be noted that the largest change in the  $I$ - $V$  curves occurs between cluster 2 ( $25 \times 8 \text{ \AA}^2$ , 150) and cluster 3 ( $28 \times 9 \text{ \AA}^2$ , 215 atoms), where the onset of the nonmetal to metal transition begins; the transition is complete by cluster 4 ( $34 \times 11 \text{ \AA}^2$ , 385 atoms). The STS spectra show very little change with increasing cluster size from  $34 \times 11 \text{ \AA}^2$  for cluster 4 to  $41 \times 15 \text{ \AA}^2$  for cluster 6. These results indicate that the nonmetal to metal transition occurs over a cluster size window between 215 and 385 atoms and the bulklike electronic structure is well developed at a cluster size as small as  $34 \times 11 \text{ \AA}^2$  (385 atoms).

Although there is a relatively good correlation between the cluster size measured in the topographic scan and the band gap measured in the STS experiments, significant scattering of the data was found. This scattering is apparent in Fig. 18, which shows a plot of band gap versus cluster size. These data were acquired on various surfaces with different Pd coverages. Clearly, however, a nonmetal to metal transition is observed and occurs somewhere between a cluster size of 250–350 atoms.

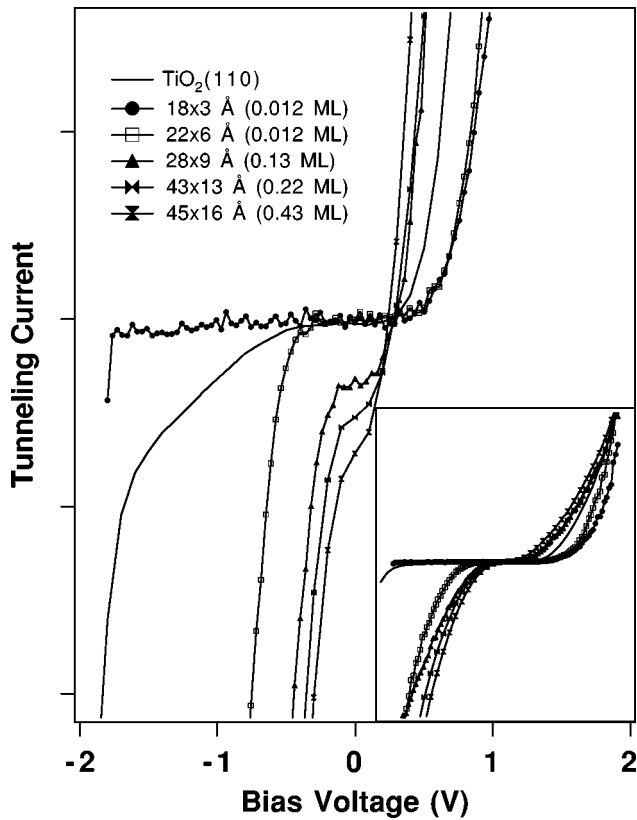


FIG. 16. STS curves of Pd clusters at various Pd coverages. The inset shows the full  $I$ - $V$  curves. The STS curves for the three largest clusters were offset for clarity.

## IV. DISCUSSION

### A. The clean $\text{TiO}_2(110)$ surface

The  $\text{TiO}_2(110)$  surface has been extensively studied previously using a variety of surface science techniques. There is general agreement about the structure of the unreconstructed  $\text{TiO}_2(110)$  surface, schematically shown in Fig. 1. In all of the scanning tunneling micrographs,<sup>11-17</sup> only one of the two surface ions (Ti and O) was imaged. Since all the images were acquired at a positive sample bias and since the density of the unoccupied states near the Fermi level is primarily located on the Ti cation, it has been assumed that the imaged cation was Ti. This assignment was verified by Onishi and Iwasawa<sup>18</sup> in a very elegant experiment. Using formate as an atomic scale marker, these authors showed that the formate species sits directly on top of the bright ridge of atoms in the STM image. Since the formate species is well known to be bound to the surface Ti cation via the formate oxygen atoms, these results provided unambiguous support for the assignment of the Ti cations as the imaged atoms in the STM experiments. However, Fischer *et al.*<sup>17</sup> have argued that oxygen is the atom imaged in the STM experiments since the oxygen anion is much closer to the STM tip and also has partially unoccupied orbitals due to the partial covalent character of the Ti-O bond. This assignment was supported by their experiments in which oxygen vacancies were created by annealing to  $>1000$  K, and an STM image then acquired. Using the same approach, but with oxygen vacancies created by annealing to 700 K, Diebold *et al.*<sup>19</sup> reached the opposite conclusion to that of Fischer *et al.*<sup>17</sup> The results of Diebold *et al.*,<sup>19</sup> are consistent with the Ti cations being

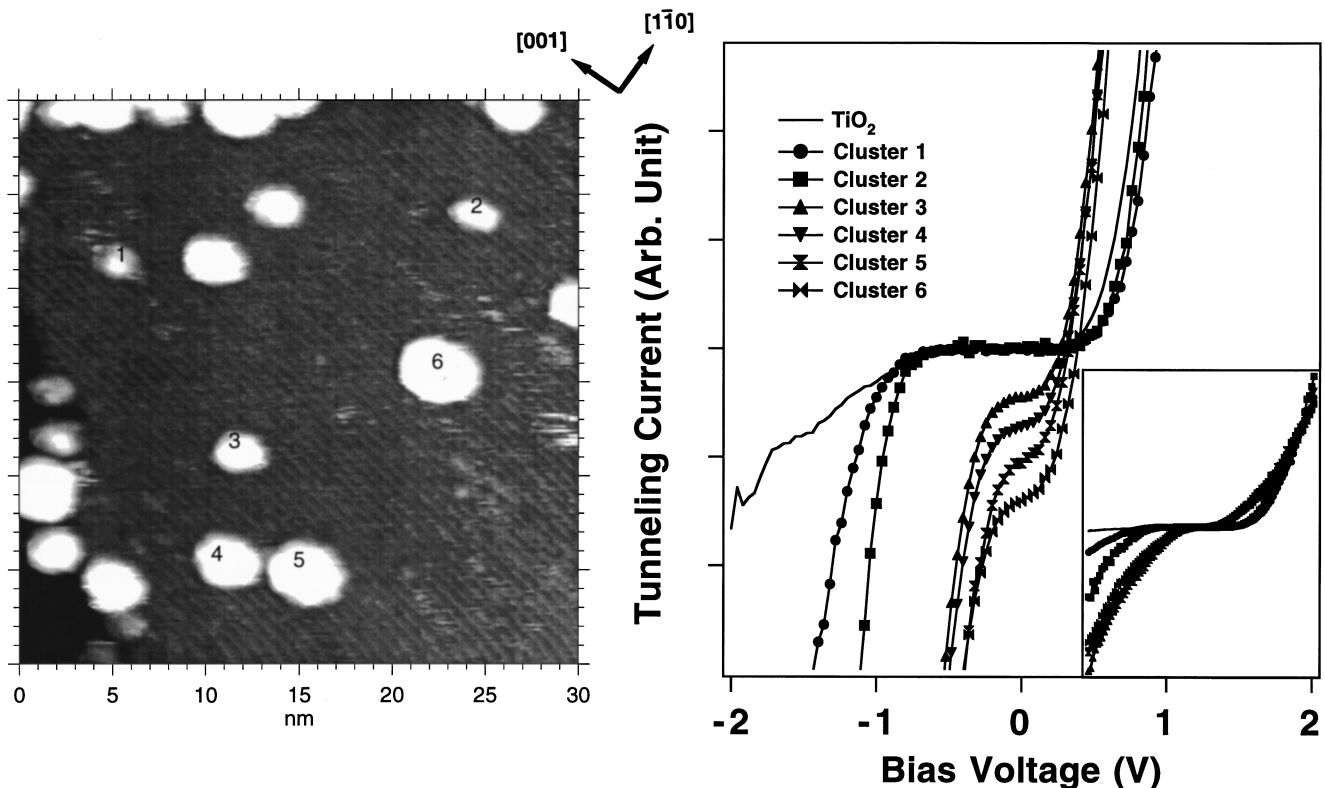
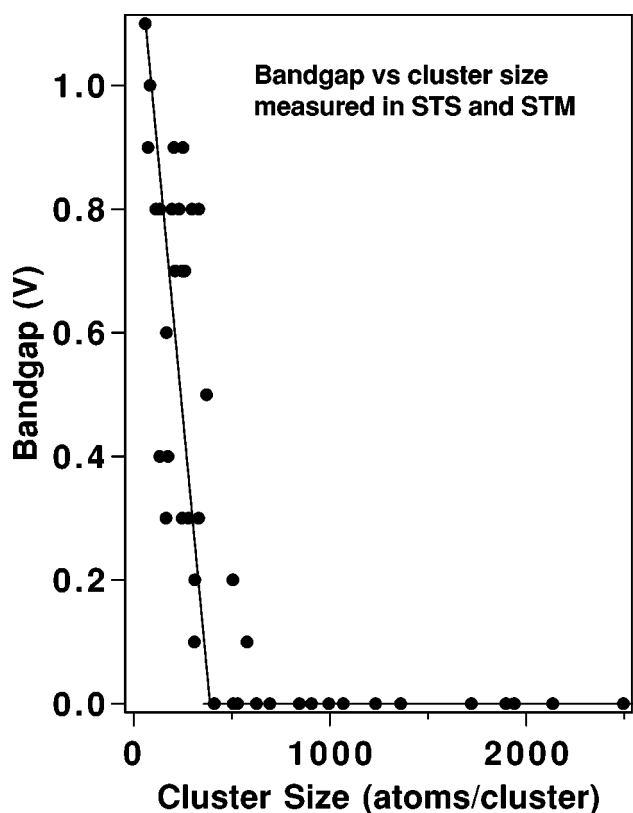


FIG. 17. STS curves for different sizes of clusters on the same  $\text{TiO}_2(110)$  surface. The corresponding topographic scan is also shown. The STS curves for clusters 3-6 were offset for clarity.



ally even at low Pd coverages. Only at the lowest Pd coverage (0.012 ML) used in our experiments, 2D clusters were observed. Structures pseudomorphic to the  $\text{TiO}_2(110)$  substrate were observed for the 2D Pd clusters, with significantly longer Pd-Pd bonds compared to bulk Pd. Apparently, the Pd-substrate interaction dominates the structure in the small 2D Pd clusters. As a consequence, the 2D Pd clusters show significantly different electronic properties compared to the 3D cluster as the STS data of Fig. 15 demonstrate.

The cluster sizes and their distribution depend strongly on the metal coverage, the metal flux, and the substrate temperature. The higher flux leads to smaller clusters and to narrower size distributions than the lower flux, apparently due to the competing processes of nucleation and growth. Consistent with the classic nucleation and growth mode,<sup>35,36</sup> only Pd dimers have been observed at the initial nucleation stage; no monomers were found. The monomer is very mobile on the surface, while the dimer is a relatively stable entity and can serve as a stable nucleation site. With increasing Pd flux, the probability of a monomer forming a dimer with an incoming Pd atom increases. The formation of a Pd dimer obviously will slow the diffusion of Pd atoms and thus Pd cluster growth. As a result, higher cluster densities and smaller clusters were observed with the higher Pd fluxes. A marked preferential nucleation of clusters at the step edges was also observed relative to the flat terrace. This can be attributed to either more strongly bound Pd at the step edge compared with Pd on the flat terrace or simply to mechanical accommodation of the Pd atoms at the step edge due to a high-diffusional barrier for Pd to move over the step.

Even at a Pd flux of 0.1 ML/min, nucleation is already a rapid process and is complete at a Pd coverage of  $\sim 0.2$  ML. Subsequent to impinging on the surface, the Pd atoms are rather mobile. Also the mean free path on the surface of Pd is significantly larger than half the average distance (40 Å) between two adjacent Pd clusters at a Pd coverage of 0.2 ML and a dosing flux of 0.1 ML/min.

Although CO adsorption does not induce any change in the structure of the Pd clusters at 300 K and a CO background pressure of  $1 \times 10^{-5}$  Torr, the presence of  $1 \times 10^{-6}$  Torr background CO during the Pd deposition has a marked influence on the nucleation and growth of Pd on the  $\text{TiO}_2(110)$  surface. CO seems to destabilize the nuclei and promote the formation of 3D clusters. CO adsorption has been previously studied by Linsebigler, Lu, and Yates<sup>37</sup> on the  $\text{TiO}_2(110)$  surface with and without oxygen vacancies. On the oxidized surface, CO desorbs in a single peak at about 150 K. However, on the  $\text{TiO}_2(110)$  surface with oxygen vacancies (created by annealing) CO desorption was observed at a temperature as high as 350 K. Therefore, the presence of background CO during the Pd deposition blocks these defect sites which otherwise will serve as a nucleation center. Thus, the cluster density is significantly reduced. Furthermore, the presence of CO also seems to reduce the barrier for Pd diffusion over the step edge and promotes Pd cluster growth in the direction parallel to the surface normal. It should be noted that our results for Pd differ significantly from the results of Steinrueck *et al.*<sup>34</sup> for Pt adsorption on the  $\text{TiO}_2(110)$  surface. These authors concluded from the rapid decrease of the substrate low-energy ion-scattering signal with increasing Pt coverage in the presence of CO compared

to that without CO that CO promotes a higher degree of wetting between Pt and  $\text{TiO}_2$ . It is unclear what causes this particular difference in these two systems. Further experiments are under way in our laboratories to address this issue.

Based on the high-resolution STM images, the initial adsorption sites for Pd on the  $\text{TiO}_2(110)$  surface are on the fivefold-coordinated Ti rows. The same adsorption site has previously been found by Schierbaum *et al.* for Pt on the  $\text{TiO}_2(110)$  surface,<sup>38</sup> and is consistent with the relatively low oxygen affinity of Pd.

The ability to perform high-quality STS measurements and to simultaneously obtain topographic images allows the determination of the electronic structure of individual metal clusters on the microscopic scale. A clear metal to nonmetal transition was observed with decreasing cluster size at  $\sim 300$  atoms/cluster. A band gap in metal clusters has been previously observed by First *et al.*<sup>39</sup> for Fe clusters on the GaAs(110) surface and by Suzuki and Fukuda<sup>40</sup> for Al clusters on the GaAs(110) surface. For Fe on GaAs(110), Fe clusters consisting of about 13 atoms show nonmetallic character, while the metallic character is fully developed for clusters consisting of more than 35 atoms. In the case of Al on GaAs(110), however, clusters consisting of as many as 200 atoms still show nonmetallic character. The size of the Pd clusters with nonmetallic character are somewhat larger than the previously reported Fe clusters with similar properties, but similar in size to the nonmetallic Al clusters. These results imply that the nonmetal to metal transition is dependent upon both the metal and the support.

## V. CONCLUSIONS

Ti cations and oxygen anions can be imaged depending on the nature of the STM tip. A low-temperature (700–800 K)  $(1 \times 2)$   $\text{TiO}_2(110)$  phase has been observed using STM and is most likely formed by recombinative oxygen desorption. This  $(1 \times 2)$  phase can be converted to the  $(1 \times 1)$  phase by annealing to between 900 and 1100 K presumably due to oxygen diffusion from the bulk to the surface.

Pd grows three dimensionally on the  $\text{TiO}_2(110)$  surface at 300 K. Only at very low Pd coverage (0.012 ML), two-dimensional Pd clusters were found. This is consistent with the rather low affinity of Pd towards oxygen. Two-dimensional Pd clusters show a structure pseudomorphic to the substrate structure and a significantly larger Pd-Pd distance compared to bulk Pd.

The initial adsorption site for Pd on the  $\text{TiO}_2(110)$  surface was found to be the fivefold-coordinate Ti rows. There is a marked preferential nucleation of Pd clusters at step edges.

Only dimers and tetramers have been observed; no monomers were found. This is consistent with the classical model of metal nucleation and growth on oxide surfaces, which assumes that only monomers are mobile and that dimers are the stable nuclei. The cluster size, measured with an STM tip exhibiting atomic resolution, is in agreement with the actual cluster size, indicating a negligible electronic or tip convolution effect on the cluster size under our experimental conditions.

Although CO adsorption does not induce a reconstruction of the Pd clusters, the presence of  $1 \times 10^{-6}$  Torr CO inhibits

cluster nucleation and promotes cluster growth by “titration” of oxygen defects.

The electronic structure of individual metal clusters can be measured on the microscopic scale. The corresponding topographic scan can be used to correlate the STS curve with a particular geometric feature and, as well, provide a check for tip stability during the measurements. The nonmetal to metal transition of the Pd clusters occurs at a cluster size between 250 to 350 atoms per cluster and corresponds ap-

proximately to the transition from the 2D to 3D cluster growth mode.

#### ACKNOWLEDGMENTS

We acknowledge with pleasure the support of this work by the Department of Energy, Office of Basic Sciences, Division of Chemical Sciences, the National Science Foundation, and the Robert A. Welch Foundation.

\*Also at: Amoco Corporation, Naperville, IL 60566.

<sup>†</sup>Author to whom correspondence should be addressed.

<sup>1</sup>A. Fujishima and K. Honda, *Nature (London)* **37**, 238 (1972).

<sup>2</sup>S. J. Tauster, S. C. Fung, and R. L. Garten, *J. Am. Chem. Soc.* **100**, 170 (1978).

<sup>3</sup>P. W. Murray, F. M. Leibsle, C. A. Murny, H. J. Fisher, C. F. J. Flipse, and G. Thornton, *Phys. Rev. Lett.* **72**, 689 (1994).

<sup>4</sup>P. W. Murray, F. M. Leibsle, C. A. Murny, H. J. Fisher, C. F. J. Flipse, and G. Thornton, *Surf. Sci.* **321**, 217 (1994).

<sup>5</sup>G. W. Clark and L. L. Kesmodel, *Ultramicroscopy* **41**, 77 (1992).

<sup>6</sup>P. W. Murray, J. Shen, N. G. Condon, S. J. Pang, and G. Thornton, *Surf. Sci.* **380**, L455 (1997).

<sup>7</sup>G. E. Poirier, B. K. Hance, and J. M. White, *J. Vac. Sci. Technol. B* **10**, 6 (1992).

<sup>8</sup>G. S. Rohrer, V. E. Henrich, and D. A. Bonell, *Science* **250**, 1239 (1990).

<sup>9</sup>G. S. Rohrer, V. E. Henrich, and D. A. Bonell, *Surf. Sci.* **278**, 146 (1992).

<sup>10</sup>Q. Zhong, J. M. Vohs, and D. A. Bonnell, in *Interface Dynamics and Growth*, edited by K. S. Liang *et al.*, MRS Symposium Proceedings No. 237 (Materials Research Society, Pittsburgh, 1992), p. 453.

<sup>11</sup>M. Sander and T. Engel, *Surf. Sci. Lett.* **302**, L263 (1994).

<sup>12</sup>D. Novak, E. Garfunkel, and T. Gustafsson, *Phys. Rev. B* **50**, 5000 (1994).

<sup>13</sup>H. Onishi and Y. Iwasawa, *Surf. Sci.* **313**, L783 (1994).

<sup>14</sup>A. Szabo and T. Engel, *Surf. Sci.* **329**, 241 (1995).

<sup>15</sup>H. Onishi, K. Fukui, and Y. Iwasawa, *Bull. Chem. Soc. Jpn.* **68**, 2447 (1995).

<sup>16</sup>P. W. Murray, N. G. Condon, and G. Thornton, *Phys. Rev. B* **51**, 10 989 (1995).

<sup>17</sup>S. Fischer, A. W. Munz, K.-D. Schierbaum, and W. Goepel, *Surf. Sci.* **337**, 17 (1995).

<sup>18</sup>H. Onishi and Y. Iwasawa, *Chem. Phys. Lett.* **226**, 111 (1994).

<sup>19</sup>U. Diebold, J. F. Anderson, K. O. Ng, and D. Vanderbilt, *Phys. Rev. Lett.* **77**, 1322 (1996).

<sup>20</sup>P. J. Möller and M. C. Wu, *Surf. Sci.* **224**, 265 (1989).

<sup>21</sup>Q. Guo, I. Cocks, and E. M. Williams, *Phys. Rev. Lett.* **77**, 3851 (1996).

<sup>22</sup>H. Poppa, *Vacuum* **34**, 1081 (1984).

<sup>23</sup>D. W. Goodman, *Chem. Rev.* **95**, 523 (1995).

<sup>24</sup>V. E. Henrich and P. A. Cox, *The Surface Science of Metal Oxides* (Cambridge University Press, Cambridge, 1994).

<sup>25</sup>J. Evans, B. E. Hayden, and G. Lu, *Surf. Sci.* **360**, 61 (1996).

<sup>26</sup>T. E. Madey, in *The Chemical Physics of Solid Surfaces and Heterogeneous Catalysis*, edited by D. A. King and D. P. Woodruff (Elsevier, Amsterdam, 1997), Vol. 8.

<sup>27</sup>A. J. Melmed, *J. Vac. Sci. Technol. B* **9**, 601 (1991).

<sup>28</sup>R. Wiesendanger, *Scanning Probe Microscopy and Spectroscopy: Methods and Applications* (Cambridge University Press, Cambridge, 1994).

<sup>29</sup>A. Wawro, R. Czajka, A. Kasuya, and Y. Nishina, *Surf. Sci.* **365**, 503 (1996).

<sup>30</sup>C. Xu, X. Lai, and D. W. Goodman, *Faraday Discuss.* **105**, 247 (1996).

<sup>31</sup>M. Dorogi, J. Gomez, R. Osifchin, R. P. Andres, and R. Reifenberger, *Phys. Rev. B* **52**, 9071 (1995).

<sup>32</sup>K. H. Ernst, A. Ludviksson, R. Zhang, J. Yoshihara, and C. T. Campbell, *Phys. Rev. B* **47**, 13 782 (1993).

<sup>33</sup>A. Ludviksson, K. H. Ernst, R. Zhang, and C. T. Campbell, *J. Catal.* **141**, 380 (1993).

<sup>34</sup>H. P. Steinrueck, F. Pesty, L. Zhang, and T. E. Madey, *Phys. Rev. B* **51**, 2427 (1995).

<sup>35</sup>A. A. Schmidt, H. Eggers, K. Herwig, and R. Anton, *Surf. Sci.* **349**, 301 (1996).

<sup>36</sup>H. Poppa, *Catal. Rev. Sci. Eng.* **35**, 359 (1993).

<sup>37</sup>A. Linsebigler, G. Lu, and J. T. Yates, Jr., *J. Chem. Phys.* **103**, 9438 (1995).

<sup>38</sup>K. D. Schierbaum, S. Fischer, M. C. Torquemada, J. L. de Segovia, E. Roman, and J. A. Martin-Gago, *Surf. Sci.* **345**, 261 (1996).

<sup>39</sup>P. N. First, J. A. Stroschio, R. A. Dragoset, D. T. Pierce, and R. J. Celotta, *Phys. Rev. Lett.* **63**, 1416 (1989).

<sup>40</sup>M. Suzuki and T. Fukuda, *Phys. Rev. B* **44**, 3187 (1991).